

Spatial Bayesian Hierarchical Modelling with Integrated Nested Laplace Approximation

Nicoletta D'Angelo · Antonino
Abbruzzo · Giada Adelfio

Received: date / Accepted: date

Abstract We consider latent Gaussian fields for modelling spatial dependence in the context of both spatial point patterns and areal data, providing two different applications. The inhomogeneous Log-Gaussian Cox Process model is specified to describe a seismic sequence occurred in Greece, resorting to the Stochastic Partial Differential Equations. The Besag-York-Molli model is fitted for disease mapping of the Covid-19 infection in the North of Italy. These models both belong to the class of Bayesian hierarchical models with latent Gaussian fields whose posterior is not available in closed form. Therefore, the inference is performed with the Integrated Nested Laplace Approximation, which provides accurate and relatively fast analytical approximations to the posterior quantities of interest.

Keywords Integrated Nested Laplace Approximation; Besag-York-Molli model; Log-Gaussian Cox Process; Spatial Point Process; Disease Mapping; Covid-19

1 Introduction

The fast-growing availability of vast sets of georeferenced data has generated a keen interest in suitable statistical modelling approaches to handle large and complex data. Bayesian hierarchical models have become a vital tool for capturing and explaining complex stochastic structures in spatial or spatio-temporal processes. Many of these models are based on latent Gaussian models, a vast and exible class ranging from generalized linear mixed to spatial and

Corresponding author: Nicoletta D'Angelo, E-mail: nicoletta.dangelo@unipa.it

Nicoletta D'Angelo¹, Antonino Abbruzzo¹, Giada Adelfio^{1,2}

1- Dipartimento di Scienze Economiche, Aziendali e Statistiche, Università degli Studi di Palermo, Palermo, Italy

2- Istituto Nazionale di Geofisica e Vulcanologia (INGV), Palermo, Italy

spatio-temporal models. Generally, closed-form expressions for the posterior distributions are not available for these complex models, and Markov Chain Monte Carlo (MCMC) algorithms can be used for inference (Hastings, 1970), although this approach can be computationally demanding. Alternatively, the Integrated Nested Laplace Approximation (INLA) has been developed as a computationally efficient algorithm for making inference on latent Gaussian models (Rue et al, 2009). Combining analytical approximations and numerical integration, INLA overcomes the convergence issues of the MCMC methods, providing faster computation. However, the use of analytical approximations may introduce errors in the computation of the posterior probabilities. INLA solves inferential issues in many case studies with space-time applications. For example, it is applied to global climate data Lindgren et al (2011), in epidemiology (Bisanzio et al, 2011), in disease mapping and spread (Schrödle and Held, 2011; Schrödle et al, 2012), to air pollution risk mapping (Cameletti et al, 2013), and in econometrics (Gómez-Rubio et al, 2015). Recent review papers include Lombardo et al (2019); Cameletti et al (2019); Van Niekerk et al (2019) and the recent book of Gómez-Rubio (2020). More generally, INLA is successfully applied to generalized linear mixed models (Fong et al, 2010), log-Gaussian Cox processes (Illian et al, 2012; Gómez-Rubio et al, 2015) and survival models (Martino et al, 2011), amongst many other fields of application. The recent monograph of Blangiardo and Cameletti (2015) reviews INLA in detail and gives many practical examples (Blangiardo and Cameletti, 2015). Other available references for INLA are Moraga (2019); Krainski et al (2018); Wang et al (2018); Zuur et al (2017).

The aim of this paper is to provide a review of the most common spatial models for epidemic phenomena, by means of well established standard methods. We explore the strength of the INLA approach in modelling spatial data available at different levels of detail, i.e. individual and aggregated. According to the nature of data, different complex models are proposed in the literature. In this paper, we focus on the latent Gaussian models applied to a seismic sequence occurred in Greece from 2005 and 2014, and the disease mapping of the Covid-19 infectious in the North of Italy from February to the end of April 2020.

The first application refers to a seismic sequence described by fitting an inhomogeneous Log-Gaussian Cox Process (LGCP) model. The spatial seismic process belongs to the class of point pattern data, where the location of events in space are the observations of interest. The aim is typically to learn about the mechanism that generates these events (Møller et al, 1998; Diggle, 2013; Illian et al, 2008; Bakka et al, 2018). Different classes of point process models have been discussed in the literature, from the simplest homogeneous Poisson process, which is used to describe uniform spatial randomness, to more complex models that generate aggregated or patterns exhibiting repulsion among points (Van Lieshout, 2000; Møller, 2003; Illian et al, 2008). The seismological process is a very complex phenomenon, characterized by fractal and multi-scale structures: its description needs complex models, able to account for environmental heterogeneity and detecting interactions at several

spatial scales, usually in terms of clustering. Indeed, the distribution of seismic events is relatively complex, and different sources of earthquakes (faults, active tectonic plate and volcanoes) may produce events with different spatial displacements and orientations. The multi-scale interaction between the earthquakes and the relationship between the conditional intensity and the geological information available in the study area can be a crucial point of research (Siino et al, 2016). When dealing with point-reference data a computationally effective estimation approach is based on the Stochastic Partial Differential Equation (SPDE) method (Lindgren et al, 2011). This method consists of representing a continuous spatial process, e.g. a Gaussian Random Field with the Matrn covariance function, as a discretely indexed spatial random process, e.g. a Gaussian Markov Random Field, providing substantial computational advantages. Therefore, in this paper, we explore the advantages the LGCP fitting to the considered Greek complex seismic data, characterized by a strong clustered structure, using the SPDE models, as in Simpson et al (2016).

In the second application, the mapping of the Covid-19 infectious disease in the North of Italy, caused by the most recently discovered coronavirus, is provided by fitting the BYM model, thought the INLA estimation approach. This new virus and the triggered disease were unknown before the outbreak began in Wuhan, China, in December 2019. However, Covid-19 is still a tragic pandemic spreading out around the world very quickly. Italy is one of the most affected countries. Recent papers, dealing with the outbreak and spread of Covid-19 infectious disease, concern analyses both at country level (Kang et al, 2020) and global scale (Liao et al, 2020). These papers mostly provide descriptive analysis in terms of the geographic distribution of the Covid-19 cases. Few attempts have been made in proposing modelling approaches taking into account the spatial component of the phenomenon. For instance, in Ramírez-Aldana et al (2020) the authors study the epidemic spread in Iran through spatial linear models in order to identify the variables that have significantly impacted the number of cases of Covid-19. In this paper, we analyse the Italian data on Covid-19, which are collected at an aggregate level and comprise the daily counts of the infected people in the regions and provinces. This data is a typical example of areal data which can be modelled by the BesagYorkMolli (BYM) model Besag et al (1991). This is widely used in disease mapping based on areal data, for its ability to recover risk surfaces and identify areas of high-risk areas or hot-spots, starting from aggregated data. Therefore, in this paper, the BYM model is employed for accounting for the neighbourhood structure of the available count data, modelling the number of cases per district and identifying the high-risk areas, proving that relevant information can still be elicited dealing with aggregated data, without external covariates. Furthermore, in the proposed analysis, we explore whether there is a difference between the period preceding the lock-down and the subsequent one in terms of the risk disease.

The paper is structured as follows. A brief overview of the INLA approach is given in Section 2. In Section 3, inference on the spatial LGCP, combining

the INLA and SPDE approaches and on the Besag-York-Molli with INLA, are reported. The applications to earthquake data and disease mapping are provided in Section 4. Finally, the paper ends with a discussion in Section 5.

2 Background on the Integrated Nested Laplace Approximation

INLA is designed for making inference of *Latent Gaussian Models*, a very wide and exible class of models, ranging from generalized linear mixed to spatial and spatio-temporal models. Let $Y_i, i = 1, \dots, n$, be the response variable and assume that its distribution belongs to the exponential family, in which the linear predictor η_i can include terms of covariates in an additive way,

$$\eta_i = \alpha + \sum_{k=1}^{n_\beta} \beta_k z_{ki} + \sum_{j=1}^{n_f} f^{(j)}(w_{ji}), \quad (1)$$

where $g(\cdot)$ is the link function, $\eta_i = g(\mu_i) = g(E[Y_i])$, α is the intercept, $\boldsymbol{\beta} = (\beta_1, \dots, \beta_{n_\beta})$ are the regression parameters of covariates $z = (z_1, \dots, z_{n_\beta})$, and $f = \{f^{(1)}(\cdot), f^{(2)}(\cdot), \dots, f^{(n_f)}(\cdot)\}$ is a set of n_f functions of some covariates w that may be related to η also by a non-linear relationship. This non-linear relation can be accounted for by several statistical approaches, such as random (*iid*) effects, spatially or temporally correlated effects, smoothing splines, by varying the functional form of the $f(\cdot)$ s. In other words, this formulation can be used for a wide range of models, e.g. standard and hierarchical regressions, spatial and spatio-temporal models, etc. Let $\boldsymbol{\theta} = (\theta_1, \dots, \theta_{1+n_\beta+n_f}) = (\alpha, \boldsymbol{\beta}, f)$ denote the vector of the model parameters, called latent field, and assume that the multivariate distribution belongs to a Gaussian Markov Random Field (GMRF), with zero mean and with a sparse precision matrix $Q(\boldsymbol{\psi})$, where $\boldsymbol{\psi}$ denotes a vector of hyperparameters, which are not necessarily Gaussian. The main goal of the INLA-methodology is to obtain the marginal distributions for the elements of the latent field $p(\boldsymbol{\theta}|\mathbf{y})$ and the hyperparameters $p(\boldsymbol{\psi}|\mathbf{y})$, and use these to compute posterior summary statistics. This is achieved by exploiting the computational properties of the GMRF and the Laplace approximation for multidimensional integration, assuming the conditional independence of the observed variables \mathbf{y} given the latent field $\boldsymbol{\theta}$ and the hyperparameters $\boldsymbol{\psi}$. For further details on the inferential process we refer to Rue et al (2009); Martins et al (2013); Blangiardo et al (2013).

3 Spatial models with INLA

Spatial models can be distinguished into continuous and discrete domain models. When geocodes are available, Log-Gaussian Cox Processes (LGCPs), that are continuous domain models, can be used (Konstantinoudis et al, 2020). When individual data are not available, models for areal data can be applied. In particular, the BesagYorkMolli (BYM) model is a discrete domain model,

used for describing count data per spatial unit. Both models are widely considered in disease mapping, as calculating and visualising disease risk across space is an important exploratory tool in epidemiology. Indeed, the BYM model can be seen as a special case of the LGCP, where the relative risk is assumed to be piecewise constant within regions. Li et al (2012) presents a methodology for modelling aggregated disease incidence data with the spatially continuous LGCP, using a data augmentation step to sample from the posterior distribution of the exact locations at each step of an MCMC algorithm, and modelling the exact locations with a LGCP.

3.1 Continuous domain models for spatial point processes

A spatial point pattern N is an unordered set $\mathbf{x} = \{\mathbf{x}_1, \dots, \mathbf{x}_n\}$ of points \mathbf{x}_i where $n(\mathbf{x}) = n$ denotes the number of points, not fixed in advance. If \mathbf{x} is a point pattern and $D \subset \mathbb{R}^d$ is a region such that $|W| < \infty$ and $d = 2$, we write $\mathbf{x} \cap W$ for the subset of \mathbf{x} consisting of points that fall in W and $n(\mathbf{x} \cap W)$ for denoting the number of points of \mathbf{x} falling in W . A point process model assumes that \mathbf{x} is a realization of a finite point process N in W without multiple points. A point location in the plane is denoted by a lower case letter like \mathbf{s} . Any location \mathbf{s} can be specified by its Cartesian coordinates $\mathbf{s} = (s_1, s_2)$. The coordinates of the observed events depend on an underlying generating spatial process, which is often characterized by its intensity function $\lambda(\mathbf{s})$. The intensity function measures the average number of events per unit of space, and it could also depend on covariates and other effects. Earthquakes are a typical example of point pattern data in which one is interested in studying the spatial intensity of the seismic activity observed in a given area, and the LGCP is largely used for analysing spatial point pattern for earthquake data (Møller et al, 1998; Siino et al, 2018).

The LGCP belongs to the class of the Cox processes which are models for point phenomena that are environmentally driven and have a clustered structure. They are Poisson processes with a random intensity function depending on unobservable external factors. The point process N is said to be a Cox process driven by Λ , if the conditional distribution of the point process N given a realisation $\Lambda(\mathbf{s}) = \lambda(\mathbf{s})$ is a Poisson process on W with intensity function $\lambda(\mathbf{s})$. Therefore, given an observed point pattern \mathbf{y} , the LGCP model is defined as

$$\begin{aligned} \mathbf{y} | \lambda(\mathbf{s}) &\sim e^{|\mathbf{W}| - \Lambda} \prod_{\mathbf{s}_i \in \mathbf{y}} \lambda(\mathbf{s}) \\ \log(\lambda(\mathbf{s})) &= X(\mathbf{s})' \boldsymbol{\beta} + U(\mathbf{s}) \\ U(\mathbf{s}) &\sim \text{GRF}(0, \Sigma(\sigma^2, r)). \end{aligned} \quad (2)$$

Let \mathbf{s} be any location in a study area W and let $U(\mathbf{s})$ be the random spatial effect at that location. $U(\mathbf{s})$ is a stochastic process, with $\mathbf{s} \in W$, where $W \in \mathbb{R}^2$. Since $U(\mathbf{s})$ is assumed to be continuous over space, then it is a continuously-indexed Gaussian Random Field (GRF). This implies that it is

possible to collect these data at any finite set of locations within the study region. We denote by $u(s_i), i = 1, \dots, n$ a realization of $U(\mathbf{s})$ at n locations, which is assumed to have a multivariate Gaussian distribution. Therefore, for the specification of the model, it is necessary to define its mean and covariance.

Since a zero mean process is usually assumed, its multivariate distribution is completely determined by the spatial covariance function. The range parameter r of the spatial covariance function controls the roughness of the relative risk surface, i.e. larger values provide stronger correlation and smoother surfaces, while σ^2 is the marginal variance of the process. The LGCP model allows to account for further additive external covariates. In the context of spatial point processes, the $X(\mathbf{s})$ are referred to as spatial covariates, meaning that their value is assumed to be observable, at least in principle, at each location \mathbf{s} in the window W . For inferential purposes, their values must be known at each point of the data point pattern and at least at some other locations. In this LGCP model specification, the latent field is represented by $\boldsymbol{\theta} = (\boldsymbol{\beta}, \mathbf{u})$ and the hyperparameters are $\boldsymbol{\psi} = (\sigma^2, r)$.

In general, the Cox model is estimated by a two-step procedure, involving first the intensity and then the cluster or correlation parameters. In the first step, a Poisson model with the same model formula is fitted to the point pattern data, providing the estimates of the coefficients of all the terms in the model formula that characterize the intensity. Then, in the second step, the estimated intensity is taken as the true one and the cluster or correlation parameters are estimated by the method of minimum contrast (Pfanzagl, 1969; Eguchi, 1983; Diggle, 1979; Diggle and Gratton, 1984; Siino et al, 2018), or the Palm likelihood (Ogata and Katsura, 1991; Tanaka et al, 2008) or composite likelihood (Guan, 2006).

Unlike traditional inferential methods for the LGCP models, the SPDE approach uses the exact locations of the point pattern and provides a continuous approximation of the latent field. In the case of geostatistical data, $U(\mathbf{s})$ has a multivariate Normal distribution with zero mean and spatially structured covariance matrix Σ , whose generic elements is $\Sigma_{ij} = \sigma^2 Cov(U(s_i), U(s_j))$ where

$$Cov(U(s_i), U(s_j)) = \frac{1}{\Gamma(\nu)2^{\nu-1}} (\kappa \Delta_{ij})^\nu K_\nu(\kappa \Delta_{ij}) \quad (3)$$

is the isotropic Matrn spatial covariance function (Cressie, 1992), depending on the Euclidean distance between the locations $\Delta_{ij} = \|s_i - s_j\|$. The parameter K_ν denotes the modified Bessel function of second kind and order $\nu > 0$, which measures the degree of smoothness of the process and is usually kept fixed. Conversely, $\kappa > 0$ is a scaling parameter related to the range r , i.e. the distance at which the spatial correlation becomes almost null. Typically, the empirically derived definition $r = \frac{\sqrt{8\nu}}{\kappa}$ is used (Lindgren et al, 2011), with r corresponding to the distance at which the spatial correlation is close to 0.1 for each ν . Other models can be considered for the spatial covariance function, but in this paper we only focus on the Matrn model since it is used in the SPDE approach proposed by Lindgren et al (2011). However, this point does not represent a limitation, since, as stated by Guttorp and Gneiting (2006),

the Matrn family is a very flexible class of covariance functions able to cover a wide range of spatial fields. In detail, the SPDE is a computationally effective tool dealing with point-reference data. It consists in representing a continuous spatial process, e.g. the GRF $U(\mathbf{s})$ with the Matrn covariance function defined in Equation (3), as a discretely indexed spatial random process (e.g. a GMRF) by a basis function representation defined on a triangulation of the domain W , that in turn, produces substantial computational advantages. We refer to Lindgren et al (2011) for a complete description. The `inlabru` package (Bachl et al, 2019) provides a simple interface for the analysis of point patterns with INLA and SPDE models. However, in the next sections we provide full details to fit the model according to Simpson et al (2016).

3.2 Discrete domain models for areal data

The Besag-York-Molli model Besag et al (1991) is an extension of the ICAR (Intrinsic Conditional Autoregressive) model, obtained by adding a spatially unstructured random effect to the already given spatially structured random effect. The latter is a realisation of a GMRF with zero mean and a sparse precision matrix capturing strong spatial dependence. The unstructured random effect may be seen as a collection of independent random intercepts for the various areal units. This specification leads to a piecewise constant risk surface which depends on the spatial unit selected and assumes uniform risk across this spatial unit. For some discussions of the scaling issues, refer to Freni-Sterrantino et al (2018); Riebler et al (2016).

Let Y_i be the random variable number of cases in the region $D_i, i = 1, \dots, n$, and E_i the corresponding expected cases count for the i -th spatial unit. The BYM model in its general form is

$$\begin{aligned} Y_i &\sim \text{Poisson}(E_i \lambda_i) \\ \log(\lambda_i) &= \alpha + X_i' \boldsymbol{\beta} + U_i \\ U_i &\sim \text{BYM}(\sigma_v^2, \sigma_\nu^2), \end{aligned} \quad (4)$$

where the linear predictor is specified on the logarithmic scale. As for the LGCP model specification, also the BYM accounts for further additive external covariates as potential risk factors. Here X_i are region level covariates (e.g. average income and education levels) with coefficients $\boldsymbol{\beta}$, and α is the intercept quantifying the average of the cases in all the n regions.

The random spatial process U_i is the sum of an independent Gaussian process ν_i with variance σ_ν^2 and a GMRF v_i with variance σ_v^2 . For each region, the value of the GMRF component depends on the average from the neighboring regions

$$v_i | v_{-i}, \sigma_v^2 \sim \text{GMRF} \left(\frac{\sum_{j \in d_i} v_j}{d_i}, \frac{\sigma_v^2}{d_i} \right), \quad (5)$$

where d_i is the number of areas which share boundaries with the i -th one. Two regions are usually defined as neighbours if they share a common border.

Using the notation of the Equation (1), $v_i = f^{(1)}(i)$ and $\nu_i = f^{(2)}(i)$ are two area-specific effects.

More in detail, the parameter ν_i represents the unstructured residual, modelled as

$$\nu_i | \sigma_\nu^2 \sim N(0, \sigma_\nu^2). \quad (6)$$

When the ratio $\sigma_\nu^2 / \sigma_v^2$ increases, the U_i 's spatial dependence increases as well, providing a smoother surface. The latent field is represented by $\boldsymbol{\theta} = (\alpha, \beta, \mathbf{u})$ and the hyperparameters are $\boldsymbol{\psi} = (\sigma_v^2, \sigma_\nu^2)$.

4 Spatial models estimation for two real datasets

In this section, we report the study of two spatial datasets, referring both to the continuous and discrete domain models, according to the nature of data. All the analyses are carried out using the R-INLA package (Rue et al, 2009; Martins et al, 2013; Blangiardo and Cameletti, 2015) of the software R (R Core Team, 2019). In particular, for the inhomogeneous Log-Gaussian Cox Process fitting tools with the SPDE, we refer to (Krainski et al, 2018, Chapter 4). For the specification of the Besag-York-Molli model with INLA, we refer to (Blangiardo and Cameletti, 2015, Chapter 6). All the codes of the carried out analyses throughout the paper are available on request.

4.1 Greek Seismicity characterization by a spatial LGCP

The original analysed data concern 1105 earthquakes occurred in Greece between 2005 and 2014. Only seismic events with a magnitude larger than 4 are considered in this study, and the analysis in this paper are marginal with respect to the time, focusing on the spatial dependence of events. Here we analyse a small spatial window, focusing on events with the most inhomogeneous behaviour. In detail, the study area is situated in the Ionian Sea, and it comprehends three of 'the Seven Islands', namely Ithaki, Kefalonia and Zakynthos, from North to South. In Figure 1, the 149 analysed earthquakes, together with plate boundary (in red) and faults (in blue), are displayed. In this area, earthquakes appear to be clustered in the Western area of Kefalonia island and South to the Zakynthos island. Since the distance from the seismic sources is expected to influence the intensity of earthquakes, the available spatial covariates are taken into account. These are the Distance from the faults (D_f) and the Distance from the plate boundary (D_{pb}), computed as the shortest Euclidean distances from the spatial location \mathbf{s} of events and the map of geological information (Baddeley et al, 2015). More in detail, the distance function of a set of points N is the mathematical function f such that, for any two-dimensional spatial location \mathbf{s} is the function value $f(\mathbf{s})$ is the shortest distance from \mathbf{s} to N . In particular, only the information about the top segment of the fault is used to compute the distances. Finally, also the spatial covariate D_{ns} , Distance from the nearest seismic source, is computed

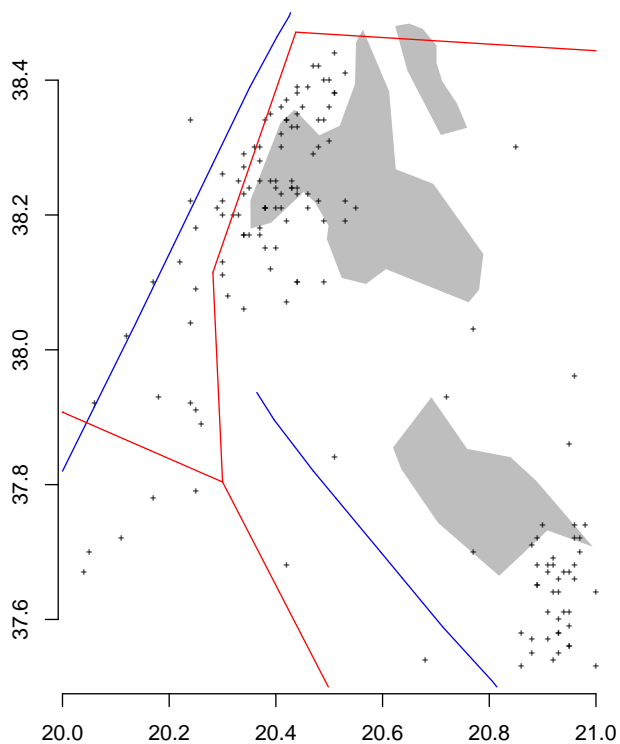


Fig. 1: Earthquakes occurred in Ithaki, Kefalonia and Zakynthos between 2005 and 2014. The plate boundary is displayed in red while the faults are displayed in blue.

and included in the analysis. The spatial covariate's surfaces are displayed in Figure 2, where a brighter colour represents a larger distance from the seismic source.

First, we fit a spatial LGCP model, without additional covariates in the linear predictor, as follows:

$$\log \lambda(s_i) = \beta_0 + u(s_i). \quad (7)$$

The SPDE approach for point pattern analysis defines the model at the nodes of the mesh, so this is built on the entire domain extent, with the largest allowed triangle edge length equal to 0.1 for the interior edges and 0.4 for the exterior (see Figure 3). Penalized Complexity priors, derived as in Fuglstad et al (2019), are used for the range r and for the standard deviation

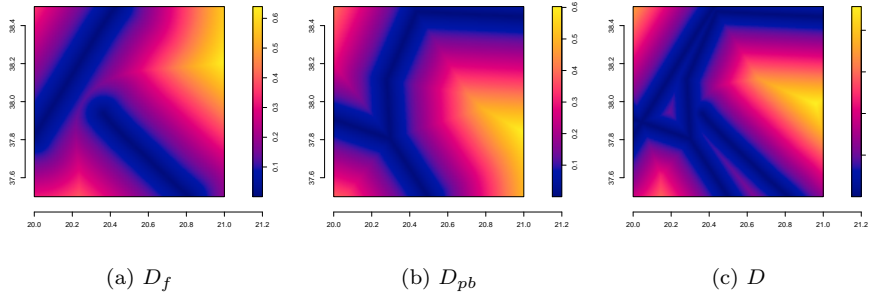


Fig. 2: Spatial covariate's surfaces

Table 1: Summary statistics of the parameters and hyperparameters of the LGCP model 7

	mean	sd	0.025quant	0.5quant	0.975quant	mode
β_0	3.40	0.92	1.42	3.45	5.15	3.53
r	0.63	0.16	0.38	0.61	0.99	0.58
σ^2	1.54	0.28	1.06	1.52	2.17	1.47

σ^2 of the Matrn covariance. In particular, the prior of the range r is set by defining (r_0, p_r) such that $P(r < r_0) = p_r$, and the the penalized complexity prior for the standard deviation σ is defined by the pair (σ_0, p_s) , such that $P(\sigma > \sigma_0) = p_s$. As a prior assumption the probability that the range is lower than 0.05 is large (i.e., $r_0 = 0.05$ and $p_r = 0.01$) and that the probability that σ is higher than 1 is small (i.e., $\sigma_0 = 1$ and $p_s = 0.01$).

The posterior distributions of the parameters and hyperparameters of the model in Equation (7) are shown in Figure 4. The summary statistics of the posterior distribution of the intercept β_0 , that in this context represents the expected number of points in the unit area, are reported in Table 1, together with the summary statistics of the posterior distributions of the hyperparameters r and σ^2 .

Then, several more complex models are fitted, adding covariates to the linear predictor. These models differ only for the specification of the linear predictor. We consider

$$\log \lambda(s_i) = \beta_0 + \beta_1 D_{ns} + u(s_i) \quad (8)$$

$$\log \lambda(s_i) = \beta_0 + \beta_1 D_f + \beta_2 D_{pb} + u(s_i) \quad (9)$$

$$\log \lambda(s_i) = \beta_0 + \beta_1 D_f + \beta_2 D_{pb} + \beta_3 D_f D_{pb} + u(s_i) \quad (10)$$

The DIC criterion (Spiegelhalter et al, 2002) and CPO values are used for comparing the estimated models, as reported in Table 2. On the one hand, the DIC is a generalization of the AIC and therefore the preferred models have low DIC values. On the other hand, the CPO estimates the probability

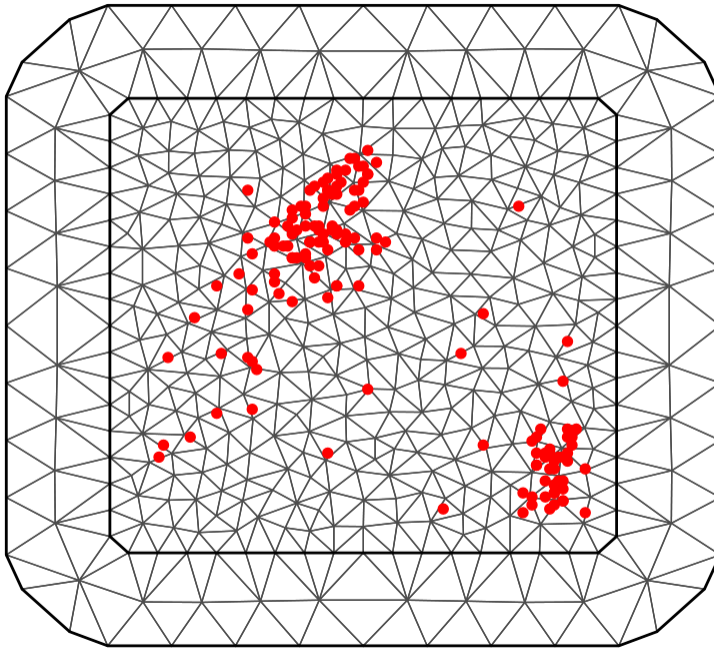


Fig. 3: Mesh used to fit the Log-Gaussian Cox Process model to the analysed point pattern

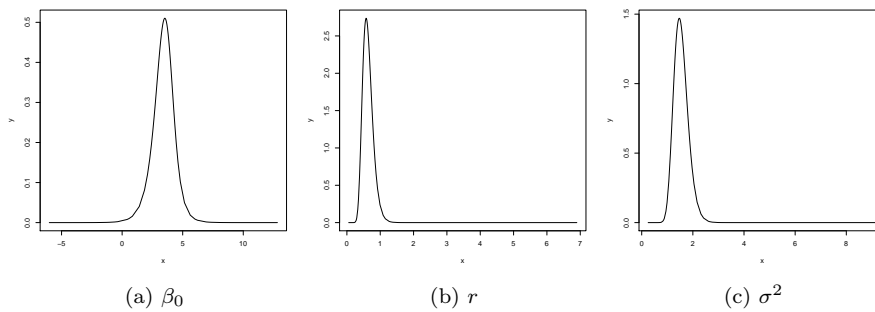


Fig. 4: Posterior distributions of the parameters and hyperparameters of the fitted LGCP model 7

Table 2: DIC and CPO values for the fitted LGCP models

	Models			
	7	8	9	10
DIC	-1509.89	-1512.20	-1514.50	-1514.81
CPO	-671.85	-649.26	-615.90	-595.40

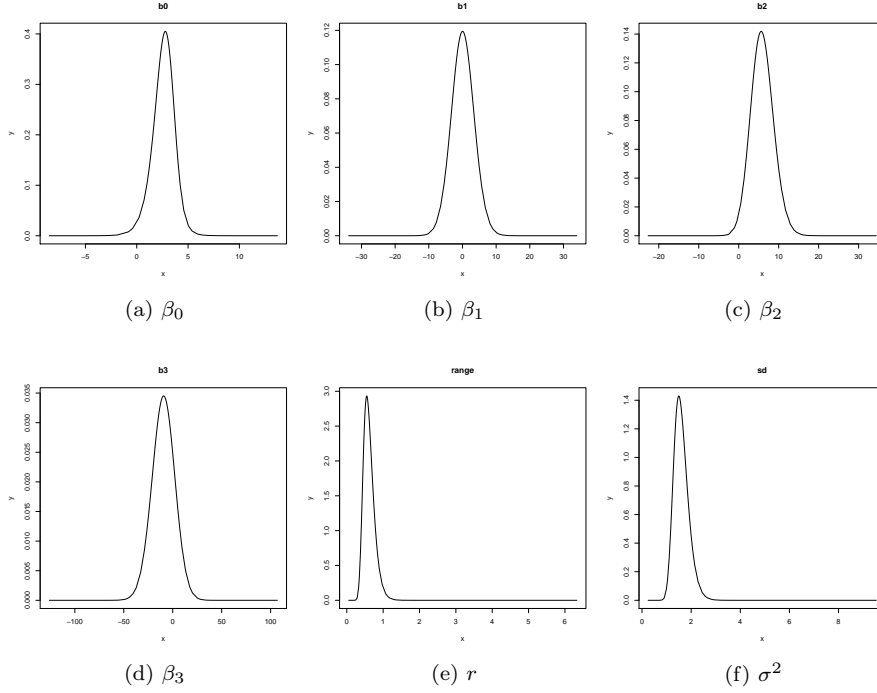


Fig. 5: Posterior distributions of the parameters and hyperparameters of the fitted LGCP model 10

of observing y_i in the future after having already observed y_{-i} , and therefore we chose the models with high CPO values.

Given that, the selected model is the one in Equation (10), where the distances from the two different sources are taken separately, together with their interaction term. The posterior distributions of the parameters and hyperparameters of this model are shown in Figure 5, and their summary statistics are reported in Table 3.

The posterior distributions of the hyperparameters r and σ^2 , and their summary statistics, are not much different from the ones fitted in the model 7 and the other models, not reported here for brevity. On the basis of these results, $\lambda(\mathbf{s})$ suddenly changes over the study window, around its mean, that is the clustered structure of the point pattern is properly identified by the

Table 3: Summary statistics of the posterior distributions of parameters and hyperparameters of the LGCP model 10

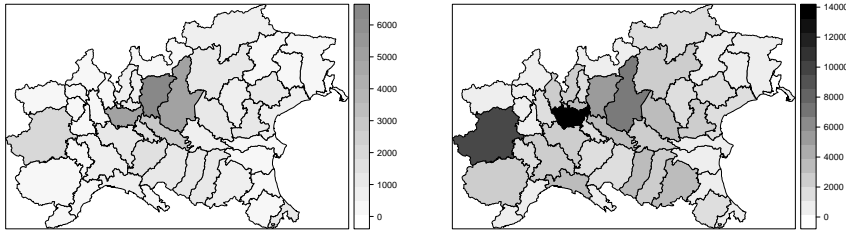
	mean	sd	0.025quant	0.5quant	0.975quant	mode
β_0	2.60	1.09	0.23	2.66	4.58	2.79
β_1	0.09	3.38	-6.52	0.06	6.81	0.03
β_2	5.88	2.85	0.52	5.79	11.72	5.62
β_3	-9.56	11.65	-32.76	-9.47	13.06	-9.27
r	0.61	0.15	0.38	0.59	0.97	0.55
σ^2	1.60	0.30	1.11	1.57	2.28	1.50

fitted model. Furthermore, looking at the summary statistics of the posterior distributions of the parameters in Table 3, we notice that the negative sign of the interaction term parameter β_3 suggests, as expected, that moving away from a seismic source the probability of the occurrence of an earthquake decreases. These results are coherent with those obtained fitting a LGCP model with the same inhomogeneous intensity, through the local Palm likelihood maximization in D'Angelo et al (2020), for the same seismic sequence.

4.2 Northern Italy Covid-19 disease mapping by the BYM model

The dataset analysed in this section refers to the number of people infected by the Covid-19 in the 47 Northern Italian provinces from February 24th to April 26th, 2020. The aim of this application is to investigate the incidence of the cases, i.e. the infected people per district in this area, that is also the most affected one in Italy and it is considered as one of the probable hot-spots of the spread of Covid-19 in Europe. A first exploratory analysis is provided splitting the time frame into two windows. Indeed, on the 8th of March the Italian Prime Minister announced a national lock-down action, leading people to a sweeping quarantine and significantly restricting the movements of the countrys population in order to limit contagions at the epicenter of the Europes outbreak. The first effects of the quarantine on the virus diffusion can be expected after at least 14 days, and for this reason we have chosen March 22nd as the change-point in the time interval. Therefore, the first time frame ranges from February 24th, that is the day when the first infected person was detected, to March 22nd, the date from which the first effects of the lock-down were expected. We refer to this first time frame as pre-lockdown period. The second frame, that ranges from the March 23rd to April 26th, is referred to as post-lockdown period.

In detail, our analysis focuses on the eight regions in the Northern Italy, namely Aosta Valley, Piedmont, Liguria, Lombardy, Emilia-Romagna, Veneto, Friuli-Venezia Giulia and Trentino-Alto Adige/Sdtirol. The counts of the infected people are collected and published daily by the Italian Civil Protection at an aggregate level, both for the regions and the provinces. In Figure 6, the number of the infected people in the 47 provinces of the eight regions are shown. The darker the colour, the more the cases observed in the given dis-



(a) Cases recorded during the pre-lockdown period (b) Cases recorded during the post-lockdown period

Fig. 6: Total number of cases recorded per district

trict. We know that most of the observed cases before the lock-down occurred in the district of Bergamo, in Lombardy, that is also the darkest district in the map of Figure 6(a). Bergamo is indeed a sadly well known hot-spot in the Italian spread of the Covid-19. After the lock-down, the observed cases have overall increased, and most of them are recorded in the district of Milan (Figure 6(b)), meaning that most of the new infected people are detected in the closest district to Bergamo. The other most affected provinces in Lombardy are Lodi and Brescia. Outside Lombardy, the most affected district is Turin, capital of the Piedmont region.

In this application, two BYM models without external covariates (i.e. risk factors) are fitted, with the log-linear predictor specified as

$$\log \lambda_i = \alpha + v_i + \nu_i \quad (11)$$

to count data aggregated in the two time frames previously chosen: [February, 24th - March, 22nd] and [March, 23rd - April, 26th]. Therefore, we fit two separate models referring to the two different periods, hereafter denoted as pre-lockdown and post-lockdown models, respectively. According to these models, the mean number of the cases per district, in the given time frames, is modelled including an intercept, common to all the provinces, and two area specific effects. These are parametrized as $u_i = v_i + \nu_i$. Furthermore, minimally informative priors are specified on the log of the unstructured and structured precisions $\log \tau_\nu$ and $\log \tau_v$, recalling that $\tau = \frac{1}{\sigma^2}$. We model the number of cases per province, without external covariates, in order to focus on the spatial variability of the phenomenon. Different analysis including eventual risk factors could be carried out for the regional-level data, for which further information about the cases is available.

The model estimation requires the individuation of the neighbours set for each borough, starting from the shapefile with this information on all the area boundaries. Therefore, since provinces are said to be neighbours if they share a common border, and knowing that on average each district borders with 4.55 other provinces, the linking neighbour provinces are reported in Figure 7.

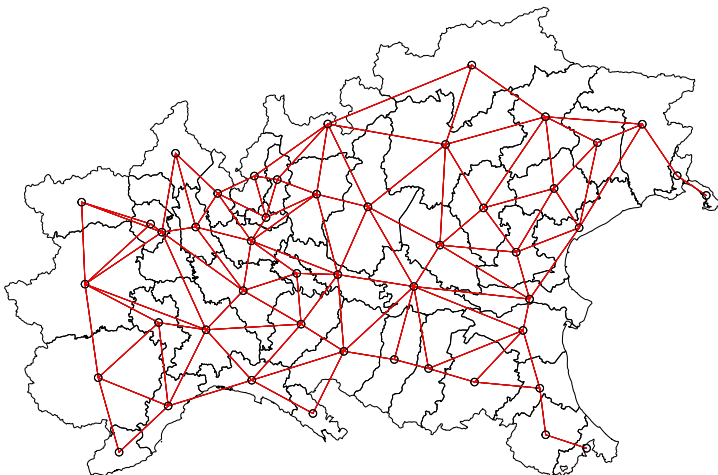


Fig. 7: Northern Italy tracts linking neighbour provinces as defined in the adjacency matrix

Table 4: Summary statistics of the parameters and hyperparameters of the pre-lockdown BYM model

	mean	sd	0.025quant	0.5quant	0.975quant	mode
α	6.32	0.12	6.07	6.32	6.57	6.32
σ_v^2	1.62	0.48	0.83	1.57	2.70	1.47
σ_v^2	1.22	0.54	0.57	1.08	2.62	0.87

The posterior distributions of the parameters and hyperparameters of the two models defined in Equation (11) are shown in Figure 8. The two hyperparameters σ_v^2 and σ_v^2 are obtained as specified in Equations (5) and (6), respectively.

The summary statistics of the posterior distribution of the intercept α , that in this context represents the expected number of cases common to all the provinces, together with the summary statistics of the posterior distributions of the hyperparameters σ_v^2 and σ_v^2 , are reported in Tables 4 and 5, for the pre- and post-lockdown models, respectively.

As far as for the BYM model, taking the exponential of the mode of the posterior distribution of α , we get the average number of counts per district, that is 561.20 with a 95% credible interval ranging from 433.71 to 714.99. The

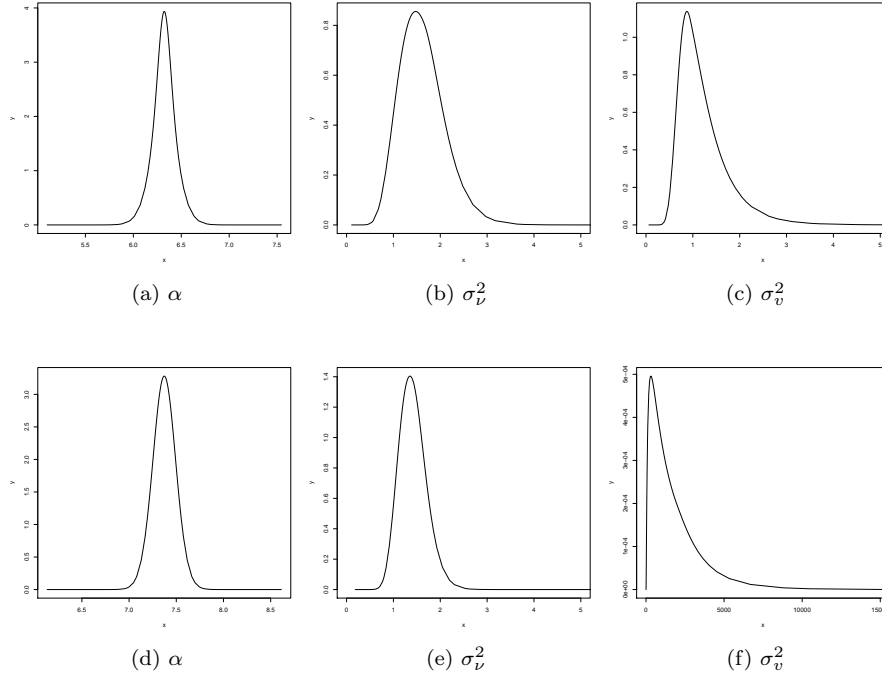


Fig. 8: Posterior distributions of the parameters and hyperparameters of the two fitted BYM models. On the top panels: the pre-lockdown BYM model ones. On the bottom panels: the post-lockdown BYM model ones.

Table 5: Summary statistics of the parameters and hyperparameters of the post-lockdown BYM model

	mean	sd	0.025quant	0.5quant	0.975quant	mode
α	7.37	0.12	7.13	7.37	7.62	7.37
σ_v^2	1.41	0.29	0.91	1.39	2.05	1.35
σ_v^2	1834.58	1835.99	116.22	1287.22	6686.58	311.80

modes of the posterior distributions of the hyperparameters are 1.47 and 0.87, for the unstructured i.i.d. and the structured spatial component, respectively.

Concerning the post-lockdown BYM model, the number of cases per district is 1604.27 with a 95% credible interval ranging from 1248.74 to 2028.56. In this case the modes of the posterior distributions of the hyperparameters are equal to 1.35 and 311.80, for the i.i.d. and the spatial component respectively.

In particular, the post-lockdown model shows an higher intercept, if compared to the pre-lockdown one. This result is reasonable, since the number of the detected cases strictly depends on the number of taken swabs, that is largely increased from the beginning of the Italian medical emergency. More-

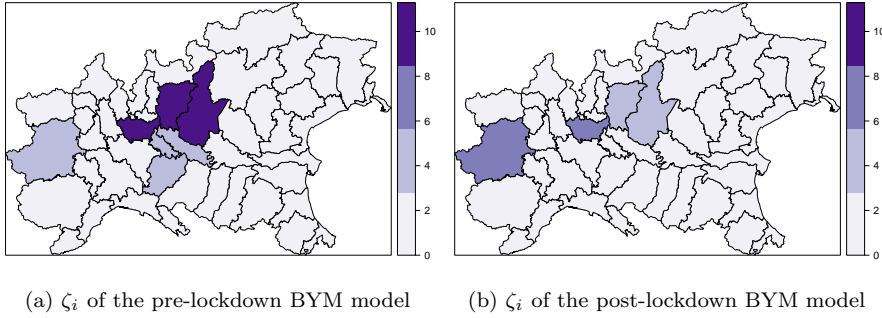


Fig. 9: District specific relative risks of cases $\zeta_i = \exp(v_i + \nu_i)$ in the disease mapping models

over, the post-lockdown model also provides an higher estimate of the mode of the posterior distribution of the precision parameter of the unstructured component, and a lower estimate of the spatial structured component, if compared to those estimated through the pre-lockdown model.

The posterior means of the random effects v_i and ν_i can be mapped, providing useful information (Richardson et al, 2004). Figure 9 shows the map of the posterior means for the district-specific relative risk of detecting cases $\zeta = \exp(\mathbf{v} + \boldsymbol{\nu})$, compared to the whole of the Northern Italy, of the two models. The darker the area, the higher the risk of infection in the given district. We may notice that in the pre-lockdown BYM model the most risk exposed provinces are those that have experienced a higher number of cases, together with some neighbour provinces, namely Milan, Bergamo and Brescia with a relative risk higher than 8, and Turin, Lodi, Cremona and Piacenza with a relative risk higher than 5. Moreover, although in the post-lockdown some provinces still have an high relative risk of cases, the overall risk is lower than the risk observed in the pre-lockdown period.

In this application the DIC values are equal to 477.49 and 526.96 for the pre-lockdown and the post-lockdown BYM models, respectively. In this particular BYM model specification, the proportion of the variance explained by the structured spatial component can be evaluated. Since σ_v^2 and σ_ν^2 are not directly comparable, we need first to get an estimate of the posterior marginal variance for the structured effect empirically, by:

$$s_v^2 = \frac{\sum_{i=1}^n (v_i - \bar{v})^2}{n - 1}, \quad (12)$$

where \bar{v} is the average of \mathbf{v} . Therefore, following Blangiardo and Cameletti (2015), the percentage of the variance explained by the structured spatial component is obtained as the ratio between s_v^2 in (12) and $s_v^2 + \sigma_\nu^2$, with σ_ν^2 the posterior marginal variance of the unstructured effect.

This percentage is 0.42 for the pre-lockdown BYM model and 0.03 for the post-lockdown one, suggesting that, while for the pre-lockdown model, a considerable part of the variability is explained by the structured spatial component, that does not hold for the post-lockdown model. Overall, the spatial structure of the pre-lockdown BYM model explains more variability than the corresponding one of the post-lockdown BYM model.

These results are coherent with the hypothesis that, after the lock-down, the spread of the Covid-19 does not seem to be mainly related to the spatial displacement of the provinces anymore, since the number of people moving among provinces has massively decreased in this second phase. However, the overall increase of the cases among the provinces may be rather caused by those district's specific issues accountable by a different class of models, operating at individual scale, rather than an aggregated one as the BYM model.

5 Discussion and conclusion

In this paper we show some peculiarities of different complex spatial models, together with the strength of the INLA approach, by considering two different, though interesting, applications.

First, we describe a spatial seismic point pattern, focusing on a sequence of seismic events in Greece. First, a LGCP model, without external covariates, is considered, where the intensity of the process only depends on the underlying spatial Gaussian Random Field. The results confirm the hypothesis that the clustered structure of the point pattern, and therefore the interaction among points, can be identified and well described by the covariance parameters. Furthermore, accounting for the available external covariates, we show that the intensity of the given process can also depend on the distance from external factors, as the seismic sources. In particular, the probability of the occurrence of an earthquake decreases when moving away from a seismic source. More in detail, results confirm that the two considered seismic sources have different effects on the intensity of the process, and also their interaction significantly characterizes the seismic generating process. Finally, we find that the INLA-based inference, also providing the posterior distribution of parameters, yields to similar results as the ones based on the local parameter estimation proposed in D'Angelo et al (2020) for the description of the same seismic data. In that paper, the local distribution of parameters have also been provided, reflecting the typical multi-scale structure that characterizes the seismic phenomenon. Furthermore, since combining the INLA and SPDE approaches, it would be possible to implement both spatial and spatio-temporal models for the description of point patterns, future analyses might account for the temporal component, to provide further attempts for characterizing the complex spatio-temporal structure of the analyzed seismic process.

To explore the broad applicability of the considered framework, we also analyse the disease count data of the Covid-19 spread out the provinces of the North of Italy, fitting a Besag-York-Molli model. Indeed, since these infection

data are available as counts per spatial unit, the BYM-type model seems to be an obvious choice for describing them. In particular, we show the spatial distribution of infections before and after the lock-down governmental action. Moreover, we identify the higher-risk areas by obtaining the posterior means of the district-specific relative risk of the detected cases, finding out that the most at risk provinces are the well-known hot-spots in Lombardy, together with Turin in Piedmont. We also observe that the overall risk of infection decreases after the lock-down, confirming the efficacy of the lockdown action taken by the Italian government. The results confirms that, while before the lock-down the spread of the Covid-19 could be attributable to the spatial displacement of provinces, the same conclusion does not hold after the lock-down, since from that time, the number of people moving among provinces has largely decreased. Furthermore, the BYM model allows to account for the spatial neighbourhood structure. This issue, together with the hierarchical structure of the considered models, can be computational challenging, making the INLA approach particularly suitable in this context. As a future hint, the availability of geocoded health data would allow to study the epidemic phenomenon as a point pattern, with methods able to account for the self-exting behaviour of events, as the ones reviewed in Meyer et al (2014).

Starting from two different datasets, observed at a different levels of detail, our study aimed at showing the main advantages of using the INLA approach, that appear to be manly its flexibility in the presence of different complex statistical models such as complex processes in spatial domain, both in the discrete and in the continuous domain, and its computational efficiency.

References

- Bachl FE, Lindgren F, Borchers DL, Illian JB (2019) `inlabru`: an r package for bayesian spatial modelling from ecological survey data. *Methods in Ecology and Evolution* 10(6):760–766
- Baddeley A, Rubak E, Turner R (2015) *Spatial point patterns: methodology and applications with R*. CRC Press
- Bakka H, Rue H, Fuglstad GA, Riebler A, Bolin D, Illian J, Krainski E, Simpson D, Lindgren F (2018) Spatial modeling with `r-inla`: A review. *Wiley Interdisciplinary Reviews: Computational Statistics* 10(6):e1443
- Besag J, York J, Mollié A (1991) Bayesian image restoration, with two applications in spatial statistics. *Annals of the institute of statistical mathematics* 43(1):1–20
- Bisanzio D, Giacobini M, Bertolotti L, Mosca A, Balbo L, Kitron U, Vazquez-Prokopec GM (2011) Spatio-temporal patterns of distribution of West Nile virus vectors in eastern Piedmont Region, Italy. *Parasites and Vectors* 4(1):230, DOI 10.1186/1756-3305-4-230, URL <http://www.parasitesandvectors.com/content/4/1/230>
- Blangiardo M, Cameletti M (2015) *Spatial and Spatio-temporal Bayesian Models with R - INLA*. John Wiley - Sons

- Blangiardo M, Cameletti M, Baio G, Rue H (2013) Spatial and spatio-temporal models with r-inla. *Spatial and spatio-temporal epidemiology* 4:33–49
- Cameletti M, Lindgren F, Simpson D, Rue H (2013) Spatio-temporal modeling of particulate matter concentration through the spde approach. *AStA Advances in Statistical Analysis* 97(2):109–131
- Cameletti M, Gómez-Rubio V, Blangiardo M (2019) Bayesian modelling for spatially misaligned health and air pollution data through the inla-spde approach. *Spatial Statistics* 31:100,353
- Cressie N (1992) *Statistics for spatial data*. Terra Nova 4(5):613–617
- D'Angelo N, Siino M, D'Alessandro A, Adelfio G (2020) Local spatial log-gaussian cox processes for seismic data. Submitted
- Diggle PJ (1979) On parameter estimation and goodness-of-fit testing for spatial point patterns. *Biometrics* pp 87–101
- Diggle PJ (2013) *Statistical analysis of spatial and spatio-temporal point patterns*. CRC press
- Diggle PJ, Gratton RJ (1984) Monte carlo methods of inference for implicit statistical models. *Journal of the Royal Statistical Society: Series B (Methodological)* 46(2):193–212
- Eguchi S (1983) Second order efficiency of minimum contrast estimators in a curved exponential family. *The Annals of Statistics* pp 793–803
- Fong Y, Rue H, Wakefield J (2010) Bayesian inference for generalized linear mixed models. *Biostatistics* 11(3):397–412, DOI 10.1093/biostatistics/kxp053
- Freni-Sterrantino A, Ventrucci M, Rue H (2018) A note on intrinsic conditional autoregressive models for disconnected graphs. *Spatial and spatio-temporal epidemiology* 26:25–34
- Fuglstad GA, Simpson D, Lindgren F, Rue H (2019) Constructing priors that penalize the complexity of gaussian random fields. *Journal of the American Statistical Association* 114(525):445–452
- Gómez-Rubio V (2020) *Bayesian inference with INLA*. CRC Press
- Gómez-Rubio V, Bivand R, Rue H (2015) A New Latent Class to Fit Spatial Econometrics Models with Integrated Nested Laplace Approximations. *Procedia Environmental Sciences* 27:116–118, DOI 10.1016/j.proenv.2015.07.119, URL <http://dx.doi.org/10.1016/j.proenv.2015.07.119>
- Gómez-Rubio V, Cameletti M, Finazzi F (2015) Analysis of massive marked point patterns with stochastic partial differential equations. *Spatial Statistics* 14:179–196
- Guan Y (2006) A composite likelihood approach in fitting spatial point process models. *Journal of the American Statistical Association* 101(476):1502–1512
- Guttorp P, Gneiting T (2006) Studies in the history of probability and statistics xlix on the matern correlation family. *Biometrika* 93(4):989–995
- Hastings WK (1970) Monte carlo sampling methods using markov chains and their applications. *Biometrika* 57(1):97–109
- Illian J, Penttinen A, Stoyan H, Stoyan D (2008) *Statistical analysis and modelling of spatial point patterns*, vol 70. John Wiley & Sons

- Illian JB, Sørbye SH, Rue H (2012) A toolbox for fitting complex spatial point process models using integrated nested laplace approximation (inla). *The Annals of Applied Statistics* pp 1499–1530
- Kang D, Choi H, Kim JH, Choi J (2020) Spatial epidemic dynamics of the covid-19 outbreak in china. *International Journal of Infectious Diseases*
- Konstantinoudis G, Schuhmacher D, Rue H, Spycher BD (2020) Discrete versus continuous domain models for disease mapping. *Spatial and Spatio-temporal Epidemiology* 32:100,319
- Krainski ET, Gómez-Rubio V, Bakka H, Lenzi A, Castro-Camilo D, Simpson D, Lindgren F, Rue H (2018) Advanced spatial modeling with stochastic partial differential equations using R and INLA. Chapman and Hall/CRC
- Li Y, Brown P, Gesink DC, Rue H (2012) Log gaussian cox processes and spatially aggregated disease incidence data. *Statistical methods in medical research* 21(5):479–507
- Liao H, Marley G, Si Y, Wang Z, Xie Y, Wang C, Tang W (2020) A tempo-geographic analysis of global covid-19 epidemic outside of china. Available at SSRN 3556632
- Lindgren F, Rue H, Lindström J (2011) An explicit link between gaussian fields and gaussian markov random fields: the stochastic partial differential equation approach. *Journal of the Royal Statistical Society: Series B (Statistical Methodology)* 73(4):423–498
- Lombardo L, Opitz T, Huser R (2019) Numerical recipes for landslide spatial prediction using r-inla: a step-by-step tutorial. In: *Spatial modeling in GIS and R for earth and environmental sciences*, Elsevier, pp 55–83
- Martino S, Akerkar R, Rue H (2011) Approximate Bayesian Inference for Survival Models. *Scandinavian Journal of Statistics* 38(3):514–528, DOI 10.1111/j.1467-9469.2010.00715.x
- Martins TG, Simpson D, Lindgren F, Rue H (2013) Bayesian computing with inla: new features. *Computational Statistics & Data Analysis* 67:68–83
- Meyer S, Held L, Höhle M (2014) Spatio-temporal analysis of epidemic phenomena using the r package surveillance. arXiv preprint arXiv:14110416
- Møller J (2003) Shot noise cox processes. *Advances in Applied Probability* pp 614–640
- Møller J, Syversveen AR, Waagepetersen RP (1998) Log gaussian cox processes. *Scandinavian Journal of Statistics* 25(3):451–482
- Moraga P (2019) Geospatial health data: Modeling and visualization with R-INLA and shiny. CRC Press
- Ogata Y, Katsura K (1991) Maximum likelihood estimates of the fractal dimension for random spatial patterns. *Biometrika* pp 463–474
- Pfanzagl J (1969) On the measurability and consistency of minimum contrast estimates. *Metrika* 14(1):249–272
- R Core Team (2019) R: A Language and Environment for Statistical Computing. R Foundation for Statistical Computing, Vienna, Austria, URL <https://www.R-project.org/>
- Ramírez-Aldana R, Gomez-Verjan JC, Bello-Chavolla OY (2020) Spatial analysis of covid-19 spread in iran: Insights into geographical and structural

- transmission determinants at a province level. medRxiv
- Richardson S, Thomson A, Best N, Elliott P (2004) Interpreting posterior relative risk estimates in disease-mapping studies. *Environmental Health Perspectives* 112(9):1016–1025
- Riebler A, Sørbye SH, Simpson D, Rue H (2016) An intuitive bayesian spatial model for disease mapping that accounts for scaling. *Statistical methods in medical research* 25(4):1145–1165
- Rue H, Martino S, Chopin N (2009) Approximate bayesian inference for latent gaussian models by using integrated nested laplace approximations. *Journal of the royal statistical society: Series b (statistical methodology)* 71(2):319–392
- Schrödle B, Held L (2011) Spatio-temporal disease mapping using INLA. *Environmetrics* 22(6):725–734, DOI 10.1002/env.1065
- Schrödle B, Held L, Rue H (2012) Assessing the Impact of a Movement Network on the Spatiotemporal Spread of Infectious Diseases. *Biometrics* 68(3):736–744, DOI 10.1111/j.1541-0420.2011.01717.x
- Siino M, Adelfio G, Mateu J, Chiodi M, D'Alessandro A (2016) Spatial pattern analysis using hybrid models: an application to the hellenic seismicity. *Stochastic Environmental Research and Risk Assessment* 31:1633–1648
- Siino M, Adelfio G, Mateu J (2018) Joint second-order parameter estimation for spatio-temporal log-gaussian cox processes. *Stochastic environmental research and risk assessment* 32(12):3525–3539
- Simpson D, Illian JB, Lindgren F, Sørbye SH, Rue H (2016) Going off grid: Computationally efficient inference for log-gaussian cox processes. *Biometrika* 103(1):49–70
- Spiegelhalter DJ, Best NG, Carlin BP, Van Der Linde A (2002) Bayesian measures of model complexity and fit. *Journal of the royal statistical society: Series b (statistical methodology)* 64(4):583–639
- Tanaka U, Ogata Y, Stoyan D (2008) Parameter estimation and model selection for neyman-scott point processes. *Biometrical Journal: Journal of Mathematical Methods in Biosciences* 50(1):43–57
- Van Lieshout M (2000) Markov point processes and their applications. World Scientific
- Van Niekerk J, Bakka H, Rue H, Schenk L (2019) New frontiers in bayesian modeling using the inla package in r. arXiv preprint arXiv:190710426
- Wang X, Yue YR, Faraway JJ (2018) Bayesian regression modeling with INLA. CRC Press
- Zuur AF, Ieno EN, Saveliev AA (2017) Spatial, temporal and spatial-temporal ecological data analysis with r-inla. Highland Statistics Ltd 1